Proposed Operation Scenarios for Inter-Band Carrier Aggregation and Spatial Multiplexing Multiple Antenna System in LTE-Advanced Network

Araz Sabir Ameen*

Electrical Engineering Department, College of Engineering, University of Sulaimani, Sulaymaniyah, Kurdistan, Iraq
E-mail: araz.ameen@univsul.edu.iq

Abstract— Carrier aggregation (CA) and spatial multiplexing (SM) multiple input multiple output (MIMO) antenna systems are used in the 4G and beyond wireless systems to achieve the desired data rates. This paper investigates the performance of the inter-band CA and SM MIMO in LTE-Advanced and recommends a CA scenario that leads to both efficient use of the MIMO antenna elements and balanced transmit power of the component carriers (CCs). The study is performed in an urban environment considering many eNodeB-UE links at CCs of 800 MHz and 2.6 GHz for different combinations of single and multiple-antenna systems. An urban site-specific 3D ray-tracing tool combined with measured antenna 3D radiation patterns is used to model radio channel of eNodeB-UE links. The simulation results show dependency of the aggregated throughput performance on the number of aggregated spatial streams and cell radius. For enhanced performance, this paper recommends aggregating either 4x4 SM MIMO operating at 800 MHz with 1x1 antenna system operating at 2.6 GHz for a cell radius of 450 m or, alternatively, 4x4 SM MIMO operating at 800 MHz with 2x2 SM MIMO operating at 2.6 GHz for a cell radius of 350 m.

Keywords— LTE-advanced network; Inter-band carrier aggregation; Spatial multiplexing; Multiple antenna system.

1.   INTRODUCTION

Wireless communication standards evolved from first generation (1G), second generation (2G), and third generation (3G) to the fourth generation (4G) and the fifth generation (5G) due to the demands for high data rates applications and quality of service (QoS). The long term evolution (LTE)-Advanced system is designed to provide peak data rates of 1 Gbps and 500 Mbps in the downlink (DL) and the uplink (UL), respectively. LTE-Advanced supports flexible bandwidths of 1.4, 3, 5, 10, 15, and 20 MHz to allow cellular system deployment in different radio frequency bands. However, the LTE-Advanced deployment with 20 MHz bandwidth is not sufficient to support the target data rates. Therefore, features such as spatial multiplexing (SM) multiple input multiple output (MIMO) antenna system and carriers aggregation (CA) are included in LTE-Advanced to achieve the target data rates [1].

CA and SM MIMO techniques increase the data rate through parallel transmission of data streams. With CA, two or more fragmented spectrums are combined to obtain a wider bandwidth and increase the data rates. The term component carrier (CC) is used to refer to center frequency of each aggregated band. The communication between the base station, known as eNodeB, and the user equipment (UE) is performed simultaneously on a number of CCs. The CCs could be in the same or in different bands, resulting in three types of CA which are: intra-band contiguous, intra-band non-contiguous, and inter-band non-contiguous. The

SM MIMO technique uses multiple antenna elements at the eNodeB and the UE to transmit multiple data streams simultaneously [2].

CA is supported in different 3GPP releases of LTE-Advanced system [3]. Release 10 of LTE-Advanced can provide a maximum aggregated bandwidth of 100 MHz through aggregation of up to five times the standard LTE-Advanced bandwidth. Additional features were added to CA in releases 11 and 12 of 3GPP LTE-Advanced system. These include support for inter-band CA in time division duplex (TDD) systems with different UL-DL configuration and CA between TDD and frequency division duplex (FDD) systems which have different frame structures [3]. However, enhancements are performed in the release 13 of 3GPP LTE-Advanced system to support the concept of massive CA based on the proposal in [4]. The proposal shows massive CA of up to 32 non-contiguous CCs to obtain much larger aggregated bandwidth for heterogeneous network.

1.1. Related Works

Recent research on CA has focused on spectrum sharing among mobile network operators (MNOs) [5-7] and resource allocation (RA) [8-12]. In [5], a framework for inter operators CA (IO-CA) is proposed to obtain dynamic aggregation of the spectrum among several MNOs. An approach for inter-band IO-CA is proposed in [6] to minimize the power consumption of the cooperative MNOs.

A resource block (RB) scheduling algorithm for CA is introduced in [8]. The study in [8] assumes equal transmit power for the CCs and divided the UEs into groups according to the coverage area of the CCs. The RA algorithm investigated in [9] performs CC selection and RB scheduling. The study is performed for LTE-Advanced heterogeneous network considering CA of four non-contiguous CCs. The study in [9] shows that round robin CC selection and best channel quality information scheduling offer the highest throughput (THR) at the UEs and balance the load across the CC, but with the cost of implementation complexity.

A queuing analytical model is developed in [10] for inter-site CA between macro-cell and small cell CCs in heterogeneous network. This queuing model offloads traffic from the macro-cells to the small cells while maintaining the QoS requirements of UEs based on the probability of packet loss and the queuing delay. A rule-based CC selection algorithm per UE is proposed in [11] to increase the THR and balance the load. The proposed method determines the number and indices of CCs to be appointed to a specific UE according to collected scores of each CC based on feedback information between UE and the cell.

A practical measurement of the performance of inter-band CA is performed in [13]. The study of [13] is performed between a CC with 10 MHz bandwidth at evolved universal terrestrial radio access (EUTRA) band 5 (869 MHz – 894 MHz) and another CC with a bandwidth of 20 MHz at the EUTRA band 7 (2620 MHz - 2690 MHz) for the DL and 2x2 SM MIMO antenna system. The study of [13] shows THR comparison of the two bands in a dense city center. For equalized power spectrum density of the two aggregated CCs, the study used higher transmit power for band 7 compared to the transmit power of band 5. However, the study does not consider single and 4x4 SM MIMO antenna systems.

1.2. Objectives of the Paper

As mentioned previously, the CA studies available in the literature consider the RA problem through assigning equal transmit power [8] or equal power spectrum density [13] for the CCs. Assigning the CCs with equal transmit power leads to different coverage area for the CCs. This has a negative impact on the overall system performance and requires different radio planning for each CC. On the other hand, assigning equal power spectrum density for the CCs requires different transmit power. Higher CC frequency requires higher transmit power. Increasing the transmit power of the base station has a negative impact on the MNOs and the environment due to increased energy bills and increased CO_2 emissions, respectively [6]. Added to that, parallel operation of CA and SM MIMO requires efficient use of the spectrum and antenna resources, especially at the UE [14]. Therefore, the objectives of this paper are:

a) To study the performance of LTE-Advanced system in the DL at two different CC frequencies and different SM MIMO antenna systems. The performance is evaluated in terms of the aggregated THR and its desired probability.

b) To propose a scenario for the concurrent operation of CA and SM MIMO antenna system that results in equal transmit power and equal coverage areas for the different CCs, in addition to efficient utilization of the antenna resources.

c) To recommend a cell radius for LTE-Advanced system that provide the highest aggregated THR at most UEs location.

The study is performed for three sector circular cells with a radius of 500 m at CCs of 2.6 GHz and 800 MHz to model the inter-band CA band, CA_7-20, between EUTRA band 7 (2620 MHz-2690 MHz) and band 20 (791 MHz - 820 MHz) [15]. The study assumes parallel transmissions over both CCs. A received bit information rate (RBIR) abstraction technique is used to estimate the DL packet error rate (PER) and THR for 1x1, 2x2, and 4x4 antenna systems. Results are generated for many eNodeB-UE links assuming an interference-free and static channel scenario. Measured 3D antenna patterns for the macro-cell eNodeB and the UE are integrated with a 3D ray tracing tool to model the wireless link in an urban propagation environment in the city center of Bristol, United Kingdom.

The remainder of this paper is organized as follows: the system model is described in section 2 which includes the channel generation, signal-to-noise ratio (SNR) calculation and THR estimations at the UEs. Section 3 shows and discusses the simulation results of different CA scenarios and conclusions are drawn in section 4.

2. SYSTEM MODEL

2.1. Channel Generation

The wireless communication channels in this paper are generated using a ray tracing tool based on an urban site-specific database [16]. The database includes terrain, buildings, and foliage. The multi path components (MPCs) are modelled through identifying all possible ray paths between the transmitter and the receiver in 3D space. Within the ray tracer, 23 macro-cell eNodeBs are placed on rooftop locations in the city center of Bristol in the United Kingdom. Each eNodeB is modelled to cover a 3-sector circular shaped cell with a radius of 500 m. Within each sector, 250 UEs are scattered at street level randomly. The system is

modelled at CCs of 800 MHz and 2.6 GHz using measured eNodeB and UE antenna patterns from [17]. Equal transmit power is assumed for both CCs based on [8]. Table 1 summarizes the channel model parameters.

Table 1. System model parameters.

Parameter		Value
LTE−advanced bandwidth		10 MHz
Subcarrier space (Δf)		15 kHz
Number of subcarriers (NSC)		600
Number of OFDM symbols (NSYM)		7
Slot time (TS)		0.5 ms
CC frequency	Band 7	2.6 GHz
	Band 20	800 MHz
Environment	City	Bristol
	Area	4 km x 4.4 km
Number of eNodeBs		23
Number of sectors		3
Number of UE per sector		60
Cell radius		500 m
eNodeB transmit power		20 Watt
eNodeB antenna down-tilt		10°
Antenna System		1x1 , 2x2 , 4x4
Antenna height	eNodeB	7 m – 77 m
	UE	1.5 m
MIMO antenna elements space	eNodeB	10 x Wavelength
	UE	0.5 x Wavelength

2.2. SNR Calculation

The LTE-Advanced system is based on a macro cellular deployment. Each eNodeB is modelled to cover a 3-sectors circular cell. The average SNR in [dB] at each UE location is calculated using Eq. (1) as a function of the received total average signal power (P_{RX}) and the additive white Gaussian noise (AWGN) power (P_{AWGN}) at the UE [18].

$$[SNR]_{dB} = [P_{RX}]_{dBw} - [P_{AWGN}]_{dBw} \tag{1}$$

For each eNodeB-UE link, PRX is calculated based on the captured MPCs of that link in the ray tracing tool and P_{AWGN} is calculated using Eq. (2) [18]:

$$[P_{AWGN}]_{dBw} = 10 \, log_{10}(\mathcal{K}.T.B_N) + F_{dB} \tag{2}$$

Where $\mathcal{K}$ represents Boltzmann's constant, T is the noise temperature in Kelvin, B_N is the effective noise bandwidth that represents the product of the number of subcarriers (N_{SC}) and the subcarrier spacing (Δf), and F_{dB} is the noise figure at the UE. In this study, a 10 MHz LTE-Advanced bandwidth is assumed along with T=288 °K and F_{dB} = 9 dB [19].

2.3. THR Estimation of the UEs

The work presented in this paper is a system-level simulation study which includes many eNodeB sites, many eNodeB-UE links, two CCs, different antenna systems (see Table 1), and different modulation and coding schemes (MCS) as shown in Table 2. Such study is time consuming when performed using bit accurate physical layer simulators. However, the

RBIR technique is a computational efficient alternative to bit level simulation when studying the system level performance of orthogonal frequency division multiplexing (OFDM) based communication system [20]. The validation study of [21], performed by the author of this paper, shows an excellent agreement between bit level simulation and the RBIR abstraction results. The RBIR runs around 300 times faster on the same computing platform.

Table 2. List of MCS modes.

Modulation	Code rate	MCS	R_{MCS} for N_{SS}=1
QPSK [k=2]	1/3	1	5.6 Mbps
	1/2	2	8.4 Mbps
	2/3	3	11.2 Mbps
	4/5	4	14.44 Mbps
16 QAM [k=4]	1/2	5	16.8 Mbps
	2/3	6	22.4 Mbps
	4/5	7	26.88 Mbps
64 QAM [k=6]	2/3	8	33.6 Mbps
	3/4	9	37.8 Mbps
	4/5	10	40.32 Mbps

The channel impulse response for each eNodeB-UE link is generated using the 3D ray tracer, converted into the frequency domain, and used as the input into the RBIR simulator of the LTE-Advanced physical downlink shared channel (PDSCH) to estimate the instantaneous PER for 10 MCS modes at average SNR determined using Eq. (1). A link adaptation algorithm is applied to select the MCS mode that maximizes the *THR* of each link. The *THR* of LTE-Advanced PDSCH for a specific MCS (THR_{MCS}) is calculated using Eq. (3) as a function of the peak error free data rate (R_{MCS}) and the *PER* for the considered MCS mode (PER_{MCS}) [22].

$$THR_{MCS} = R_{MCS} (1 - PER_{MCS}) \tag{3}$$

The achievable THR (THR_A) for each eNodeB-UE link is determined using Eq. (4) from the MCS mode that produces the highest THR [22]:

$$THR_A = \text{maximum} (THR_1, THR_2, \dots \dots, THR_{10}) \tag{4}$$

The peak error free data rate for each MCS mode (R_{MCS}) can be calculated using Eq. (5) as a function of the number of spatial streams (N_{SS}), modulation order (k_m), the coding rate (R_C), the number of active subcarriers (N_{SC}), and the number of OFDM symbols (N_{SYM}) in a time slot (T_S) [22].

$$R_{MCS} = N_{SS} \cdot \frac{k_m \cdot R_C \cdot N_{SC} \cdot N_{SYM}}{T_S} \tag{5}$$

Then the maximum peak error free data rates (R_{max}) can be calculated using Eq. (6) [22].

$$R_{max} = \text{maximum} (R_1, R_2, \dots \dots, R_{10}) \tag{6}$$

For SM MIMO antenna system, (N_R x N_T) refers to an antenna system with N_R antenna elements at the receiver (UE side) and N_T antenna elements at the transmitter (eNodeB side). Therefore, the number of spatial stream (N_{SS}) can be calculated using Eq. (7) [1].

$$N_{SS} = \text{minimum} (N_T, N_R) \tag{7}$$

Accordingly, the aggregated peak error free data rate (R_{CA}) and the number of aggregated spatial streams (N_{SS}^{CA}) for two CCs can be defined using Eqs. (8) and (9), respectively.

$$R_{CA} = R_{max1} + R_{max2} \tag{8}$$

$$N_{SS}^{CA} = N_{SS1} + N_{SS2} \tag{9}$$

In Eq. (8), R_{max1} and R_{max2} can be calculated using Eq. (6) and refer to the the maximum peak error free data rates of the 800 MHz and 2.6 GHz CCs, respectively. N_{SS1} and N_{SS2} can be calculated using Eq. (7) and represent the number of spatial stream of the 800 MHz and 2.6 GHz antenna systems, respectively.

3.   SIMULATION RESULTS

This section shows the simulation results of LTE-Advanced PDSCH. The simulation is performed for 1x1, 2x2 SM MIMO, and 4x4 SM MIMO antenna systems in the city center of Bristol, United Kingdom at CCs of 800 MHz and 2.6 GHz each with 10 MHz bandwidth. Here, the term (CA N_{SS1}–N_{SS2}) refers to the CA between the 800 MHz band with (N_{R1} x N_{T1}) antenna system and the 2.6 GHz band with (N_{R2} x N_{T2}) antenna system. Table 3 lists different CA scenarios based on the antenna system of each CC. The following sub-sections show the THR result for individual CCs considering different antenna systems, followed by simulation results for the aggregated THR as cumulative distribution function (CDF) and coverage map for different CA scenario. Note that the CDF values appear on the y-axis of the figures as probability (THR < abscissa), where abscissa refers to a specific THR value on the x-axis of the CDF figures.

Table 3. List of the CA scenarios of this study.

CA Scenario	Number of aggregated spatial streams	Antenna system	
		800 MHz	2.6 GHz
CA 1-1	2	1x1	1x1
CA 2-2	4	2x2	2x2
CA 4-4	8	4x4	4x4
CA 1-2	3	1x1	2x2
CA 2-1	3	2x2	1x1
CA 1-4	5	1x1	4x4
CA 4-1	5	4x4	1x1
CA 2-4	6	2x2	4x4
CA 4-2	6	4x4	2x2

3.1.   Achievable THR of Individual CCs

Fig. 1 shows the CDF graphs of the achievable THR (THR_A) in [Mbps] for all the eNodeB-UE links in the study. It can be observed from Fig. 1 that the achievable THR increases as the number of spatial streams increases. However, the probability of the UEs to have an achievable THR less than a desired THR, $P(THR_A < \text{desired THR})$, increases (worse performance) as the number of spatial streams and the CC frequency increase (see Table 4). In this study we select a desired THR that equals 90% of R_{max}.

For example, from Table 4, 90% of R_{max} for the 1x1, 2x2, and 4x4 SM antenna systems are 36.29 Mbps, 72.58 Mbps, and 145 Mbps, respectively. Considering the 800 MHz band, 22% of the UEs enjoy an achievable THR less than the desired THR for the 1x1 antenna system. This value increases to 32% and 43% for 2x2 and 4x4 antenna systems, respectively.

Similar conclusion can be drawn for the 2.6 GHz band but with higher probabilities. This is due to the worst PER performance of SM MIMO antenna system compared to the single antenna system. Also, as the number of antenna elements increases, the inter-stream interference between the spatial streams increases. This in turn leads to an increase in the DL spatial correlation. Consequently, the THR performance of the SM MIMO system degrades compared with a single antenna system [23].

Also, it is clear from Table 4 that with the 800 MHz band, significantly more UEs enjoy the desired THR compared to the 2.6 GHz for all the antenna systems. Additionally, the achievable THR at 800 MHz is higher than that at 2.6 GHz. This is due to the relative higher total received power of the 800 MHz band compared to the 2.6 GHz band. The differences in the number of UEs that enjoy the desired THR for different antenna systems and different CCs affect the performance of CA. Therefore, the following subsections investigate the aggregated THR performance in LTE-Advanced system considering different CA scenarios.
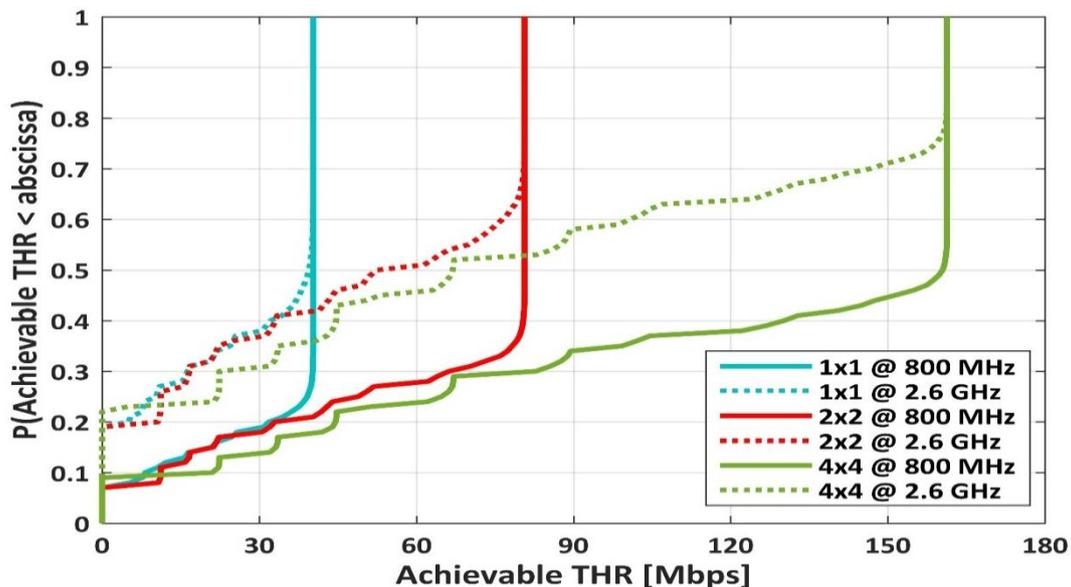

Fig. 1. CDF of UEs THR for individual CCs and antenna systems.

Table 4. Probability of (THR$_A$ < 90% R$_{max}$).

Antenna system	R$_{max}$ [Mbps]	90% R$_{max}$ [Mbps]	Probability value	
			800 MHz	2.6 GHz
1x1	40.32	36.29	22 %	43 %
2x2	80.64	72.58	32 %	57 %
4x4	161.	145	43 %	70 %

3.2. Impact of CC Selection on the Aggregated THR

This section shows the simulation results in terms of the CDF of the aggregated achievable THR. CA scenarios have the same number of aggregated spatial stream. This is to highlight the impact of CCs selection on the performance of the CA scenario. For example, the CA scenarios (CA 1-2 and CA 2-1) provide three aggregated spatial streams, but which of them provides better performance? The same comparison applies to the CA scenarios (CA1-4 with CA 4-1) and (CA 2-4 with CA 4-2), which provide five and six aggregated spatial streams, respectively as shown in Fig. 2.
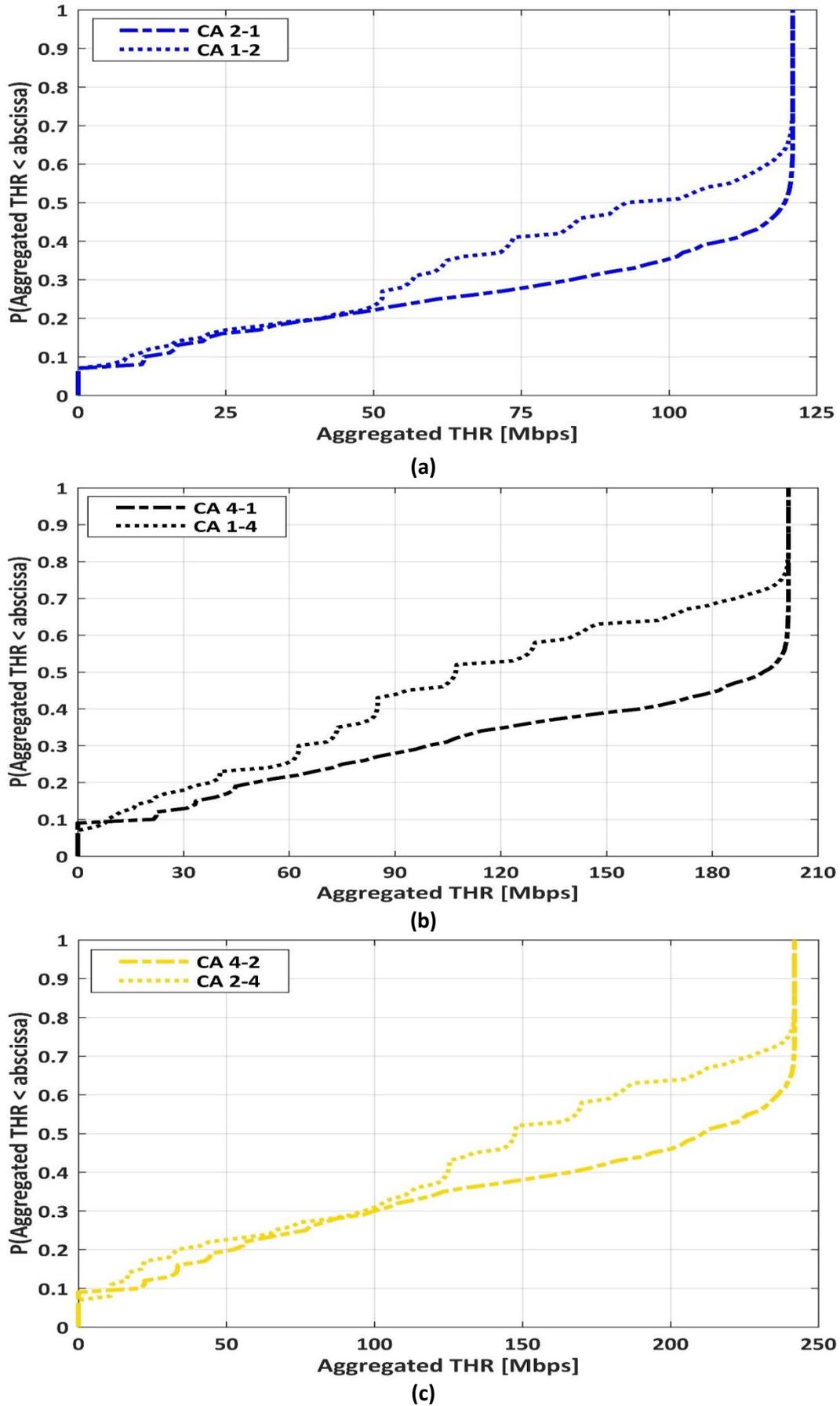
Fig. 2. CDF of UEs aggregated THR for CA scenarios with same number of aggregated spatial streams: a) three aggregated spatial streams; b) five aggregated spatial streams; c) six aggregated spatial streams.

First, consider the aggregated THR results of Fig. 2(a) which shows the results for CA scenarios with three aggregated spatial streams obtained from two different combinations of (1x1) and (2x2) SM MIMO system. It is clear from CDF graphs that CA 2-1 provides higher aggregated THR compared to CA 1-2. Next, consider the CDF graphs of Fig. 2(b) and Fig. 2(c) for five and six aggregated spatial streams, respectively. Fig. 2(b) shows that CA 4-1 provides higher aggregated THR compared to CA 1-4 and Fig. 2(c) shows better performance for CA 4-2 over CA 2-4. Hence, relatively better performance is obtained for the CA scenarios; CA 2-1, CA 4-1, and CA 4-2 over the aggregation scenarios; CA 1-2, CA 1-4, and CA 2-4.

As defined in Table 3, CA 2-1 refers to the operation of the 800 MHz with 2x2 SM MIMO and the 2.6 GHz band with 1x1 antenna system. CA 4-1 refers to the operation of the 800 MHz with 4x4 SM MIMO and the 2.6 GHz band with 1x1 antenna system CA 4-2 refers to the operation of the 800 MHz with 4x4 SM MIMO and the 2.6 GHz band with 2x2 SM MIMO antenna systems. The selection of the higher frequency CC for the SM MIMO system with lower number of spatial streams, and the lower frequency CC for the SM MIMO system with higher number of spatial streams, results in a relatively better performance. The higher received power (due to the lower pathloss) is utilized to send more spatial stream and balance the transmit power with the higher CC. Balanced transmit power results in PER enhancement by increasing SNR value of the SM MIMO. In this case, there will be efficient utilization of the antenna resources. Therefore, the following sub-sections do not include the aggregation scenarios CA 1-2, CA 1-4, and CA 2-4.

3.3.   Impact of the Number of Aggregated Spatial Streams on the Aggregated THR

This section presents the simulation results of the performance for different CA scenarios in terms of the CDFs of the achievable aggregated THR and the probability of UEs to achieve an aggregated THR less than 90% of aggregated peak error free data rate, $P(\text{aggregated } THR_A < 90\% R_{CA})$. The results show the impact of increasing the number of aggregated spatial streams on the performance of CA scenarios as shown in Table 5. Here, the scenarios include CA between CCs either operating the same antenna system (CA 1-1, CA 2-2, CA 4-4) or different antenna systems (CA 2-1, CA 4-1, CA 4-2).

Fig. 3 shows the CDFs of the aggregated THR for CA 1-1, CA 2-1, CA 2x2, CA 4-1, CA 4-2, and CA 4-4 with 2, 3, 4, 5, 6, and 8 aggregated spatial streams, respectively. As expected, the achievable aggregated THR increases as the number of aggregated spatial streams of the two CCs increases. However, as the number of the aggregated spatial streams increases, $P(\text{aggregated } THR_A < 90\% R_{CA})$ increases too. This has a negative impact on the performance and the QoS of the whole cell.

Table 5 lists the aggregated peak error free data rates, 90% of the aggregated peak error free data rates, and the $P(\text{aggregated } THR_A < 90\% R_{CA})$, as marked by black circles on the CDF graphs of Fig. 3. It is clear from Fig. 3 and Table 5 that a better performance (lower probability value) is obtained when aggregating a single antenna system but with a minimum aggregated THR. This THR can be increased by a factor of 1.5 if the single antenna system of the 800 MHz band is replaced by a (2x2) antenna system with a $P(\text{aggregated } THR_A < 90\% R_{CA})$ that equals 40%.

Fig. 3 and the data of Table 5 also indicates that the performance of the CA scenarios with five and six aggregated spatial streams outperform the performance of the CA scenario with four aggregated spatial streams in terms of aggregated THR and $P(\text{aggregated } THR_A < 90\% \, R_{CA})$. For five and six aggregated spatial streams, the 2.6 GHz band uses (1x1) and (2x2) antenna systems, respectively and the 800 MHz band uses (4x4) antenna system, while the four aggregated spatial streams are obtained when both CCs use (2x2) antenna system.

Table 5. Probability of (aggregated THR$_A$ < 90% R$_{CA}$).

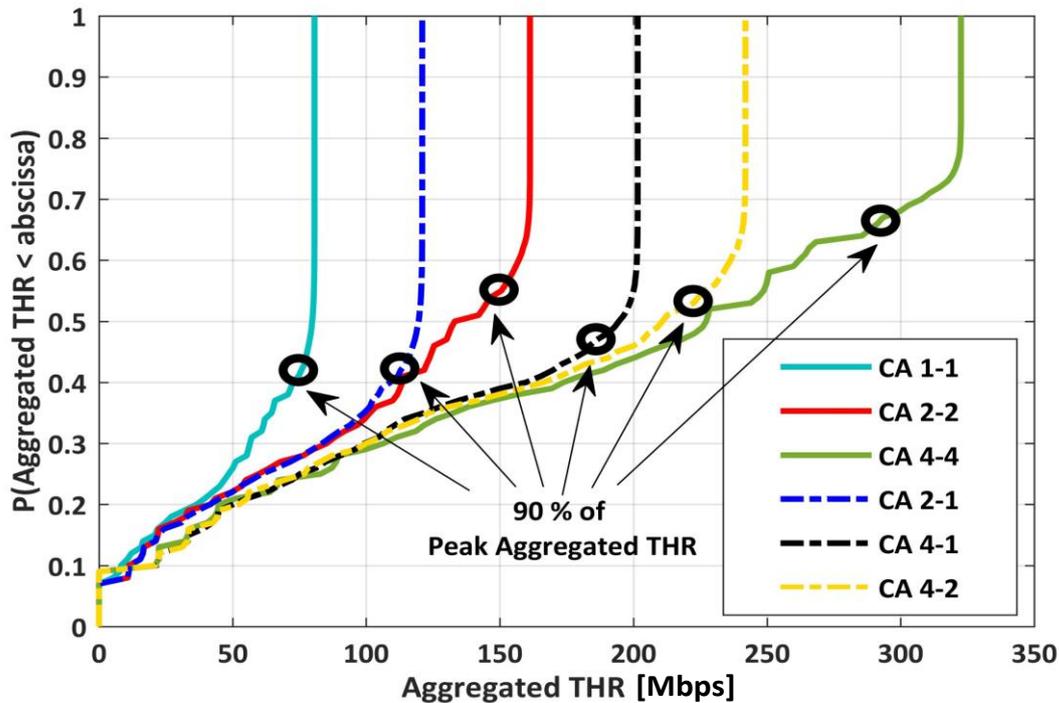| CA scenario	N$_{SS}$	R$_{CA}$ [Mbps]	90 % R$_{CA}$ [Mbps]	Probability value
CA 1-1	2	80.64	72.576	40 %
CA 2-1	3	120.96	108.864	40 %
CA 2-2	4	161.28	145.152	53 %
CA 4-1	5	201.60	181.440	45 %
CA 4-2	6	241.92	217.728	52 %
CA 4-4	8	322.56	290.304	66 %

Fig. 3. CDF of UEs aggregated THR for different CA scenarios.

3.4. Impact of the Cell Radius on the Aggregated THR

This section investigates the impact of the cell radius on the probability of achieving an aggregating THR less than a desired THR of 90% of the aggregated peak error free data rate, $P(\text{aggregated } THR_A < 90\% \, R_{CA})$. Fig. 4 shows graphs for the probability values versus the cell radii. First, consider CA 1-1 and CA 2-1. It is clear that both CA scenarios have the same probability value for all cell radiuses but with higher aggregated THR for CA 2-1. Similarly, it can be observed from the figure that the probability values of CA 2-2 and CA 4-2 are approximately the same. Therefore, CA 2-1 and CA 4-2 can be used instead of CA 1-1 and

CA 2-2, respectively to provide higher THR. For a cell radius of 500 m and CA 2-1, around 40% of the UEs enjoy an aggregated THR less than 90% of R_{CA}. This means that 60% of the UEs have aggregated THR greater than or equal to 90% of R_{CA}. These probability values can be obtained with CA 4-2 but by reducing the cell radius from 500 m to around 350 m.

Fig. 4 also shows a good performance for CA 4-1 that outperforms the performance of CA 4-2 and close to the performance of CA 2-1 in terms of probability value. The probability value of CA 2-1 at a cell radius of 500 m can be achieved with CA 4-1 by decreasing the cell to 450 m. With a reduction in the cell size by 50 m, the THR of the system can be increased by a factor of 1.6 compared to CA 2-1. CA 4-1 provides five aggregated spatial streams and CA 2-1 provides three aggregated spatial streams. Accordingly, CA 4-1 is recommended to increase the aggregated THR and provide improved QoS at most UE locations.
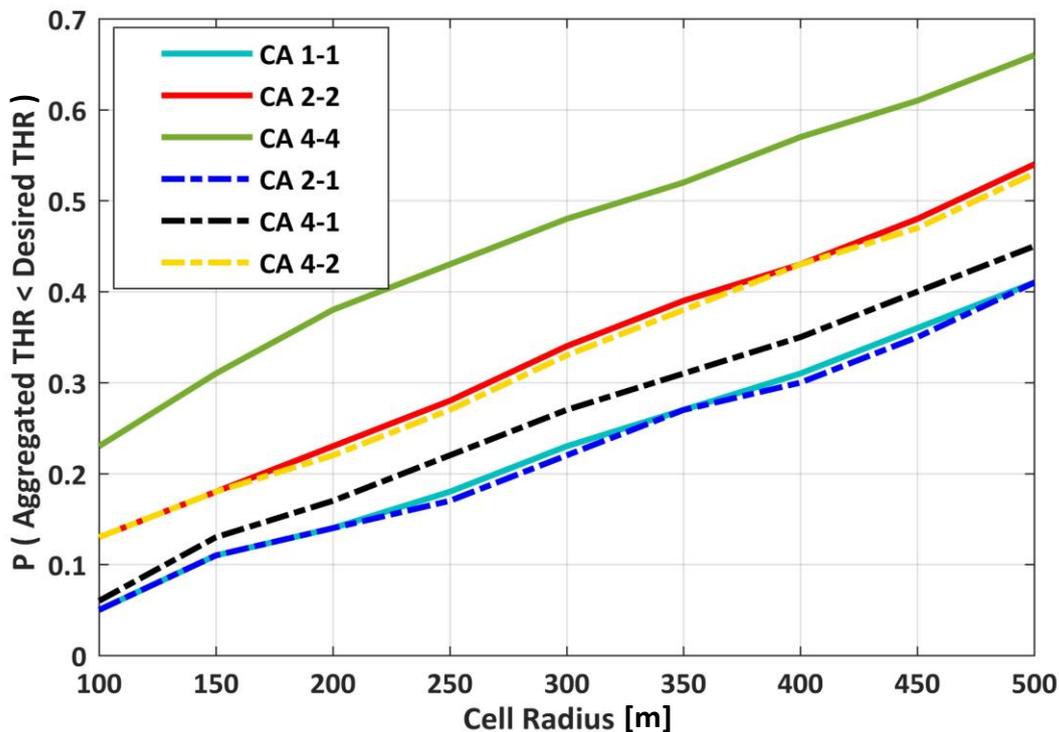

Fig. 4. Probability of achieving a desired aggregated THR versus cell radius.

3.5. Coverage Map of the Aggregated THR

This section shows the achieved aggregated THR for one cell in the city center of Bristol considering different CA scenarios. The yellow coloured points on the coverage maps of Fig. 5 refer to UE locations with an aggregated THR greater than 90% of the aggregated peak error free data rate ($aggregated\ THR_A > 90\% R_{CA}$). It is clear from Fig. 5 that CA 1-1 has more yellow coloured points compared to other CA scenarios, but with less aggregated THR. However, the number of yellow coloured points on the coverage map of CA 2-1 is very close to the coverage map of CA 1-1, but with higher aggregated THR for CA 2-1 by a factor of 1.5. The same conclusion can be drawn when comparing the coverage map of CA 2-2 with both CA 4-1 and CA 4-2 with increased aggregated THR by factors of 1.25 and 1.5 for CA 4-1 and CA 4-2, respectively. This confirms the conclusion drawn in Section 3.3.
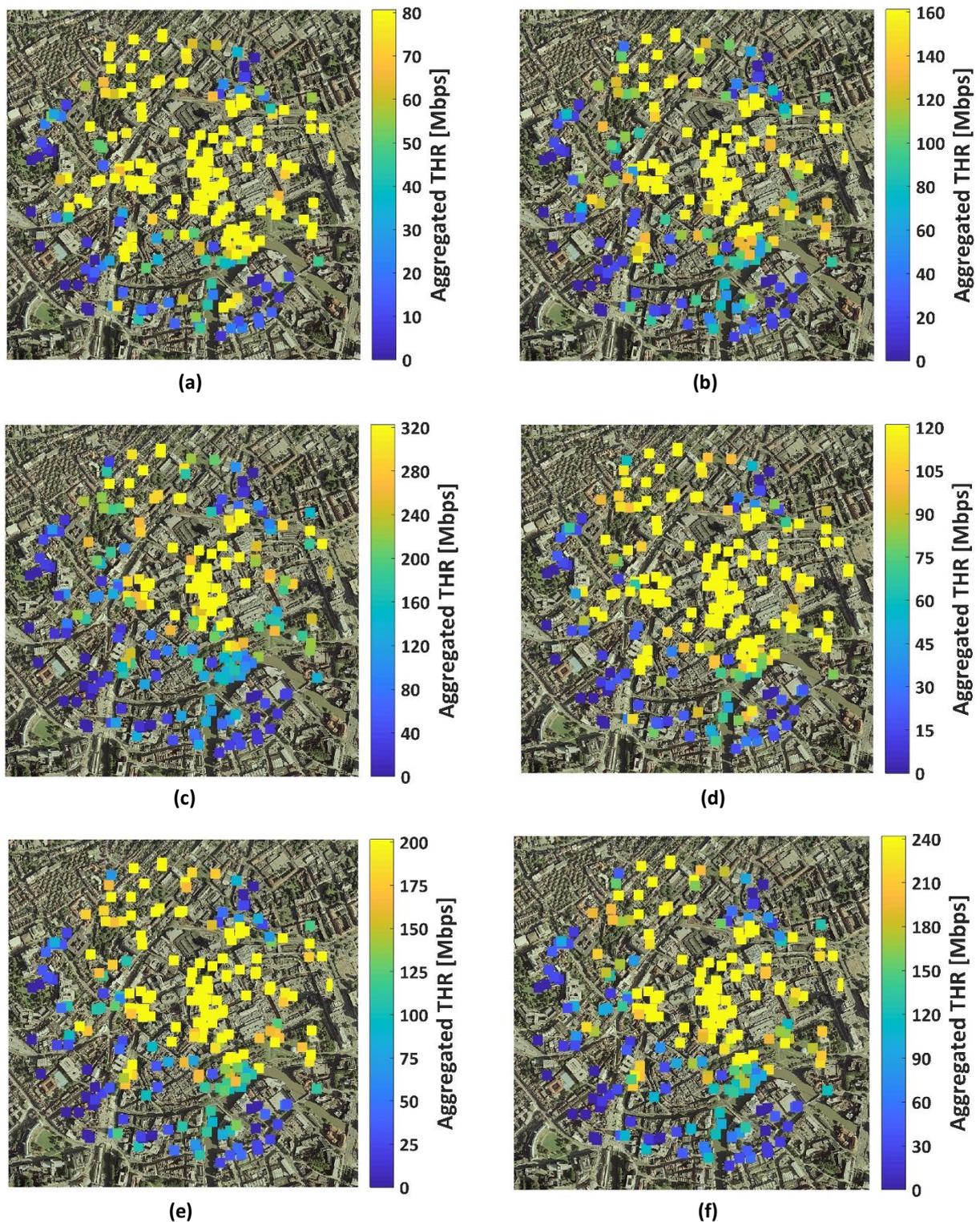
Fig. 5 Achieved aggregated THR coverage map for different CA scenarios in the city center of Bristol: a) CA 1-1; b) CA 2-2; c) CA 4-4; d) CA 2-1; e) CA 4-1; f) CA 4-2.

4.   CONCLUSIONS

This paper has evaluated the performance of LTE-Advanced physical downlink shared channel. The study was performed through system level simulation for many eNodeB-UE links in an urban environment at component carries of 800 MHz and 2.6 GHz considering different antenna systems. The radio channel of each eNodeB-UE link was modelled using

an urban site-specific 3D ray tracing tool. An RBIR abstraction model was used to estimate the PER and determine the THR at each UE location in a circular cell with a radius of 500 m.

The simulation results show dependency on the number of aggregated spatial streams and the deployed antenna system of the component carriers. Higher performance was obtained when the number of the spatial streams of 800 MHz band was higher than the 2.6 GHz band. The paper recommends a cell radius of 450 m for CA 4-1 or a cell radius of 350 m for increased aggregated THR with CA 4-2. It is important to mention that the above conclusions are based on using equal transmit power and equal coverage area for the CCs. The balance between the CCs is maintained through adjusting the number of spatial streams for each CC. This leads to efficient utilization of the antenna resources, especially at the UE. This study can be extended in the future to consider heterogeneous network and the effect of inter cell interference.

REFERENCES

[1] E. Dahlman, S. Parkvall, J. Skold, *4G LTE/LTE-Advanced for Mobile Broadband*, Oxford: Elsevier /Academic Press, 2011.

[2] D. Pehlke, K. Walsh, "LTE-advanced pro RF front-end implementations to meet emerging carrier aggregation and DL MIMO requirements," *IEEE Communication Magazine*, vol. 55, no. 4, pp. 134-141, 2017.

[3] A. Bhamri, K. Hooli, T. Lunttila, "Massive carrier aggregation in LTE-advanced pro: impact on uplink control information and corresponding enhancements," *IEEE Communications Magazine,* vol. 54, no. 5, pp. 92-97, 2016.

[4] 3GPP R1-150207, *Necessary Mechanisms and Enhancements to Support CA of up to 32 Carriers*, 2015.

[5] Y. Xiao, , Z. Han, , C. Yuen, L. DaSilva, "Carrier aggregation between operators in next generation cellular networks: a stable roommate market," *IEEE Transactions on Wireless Communications*, vol. 15, no. 1, pp. 633-650, 2016.

[6] J. Opadere, Q. Liu, T. Han, N. Ansari, "Energy-efficient virtual radio access networks for multi-operators cooperative cellular networks," *IEEE Transactions on Green Communications and Networking*, vol. 3, no. 3, pp. 603-614, 2019.

[7] S. Alja'afreh, "Folded, low profile multiband loop antenna for 4G smartphone applications," *Jordan Journal of Electrical Engineering*, vol. 2, no. 4, pp. 270-277, 2016.

[8] H. Shajaiah, A. Abdelhadi, T. Clancy, "Towards an application-aware resource scheduling with carrier aggregation in cellular systems," *IEEE Communications Letters*, vol. 20, no. 1, pp. 129-132, 2016.

[9] N. Jinaporn, S. Armour, A. Doufexi, "Performance evaluation on resource allocation with carrier aggregation in LTE cellular networks," *Proceeding of IEEE Vehicular Technology Conference*, Honolulu, HI, USA, pp. 1-5, 2019.

[10] A. Alorainy, M. Hossain, "Cross-layer performance analysis of downlink multi-flow carrier aggregation in heterogeneous networks," *IEEE Access*, vol. 7, no. 1, pp. 23303-23318, 2019.

[11] N. Mahmood, D. Laselva, D. Palacio, M. Emara, M. Filippou, D. Kim, I. Bandera, "Multi-channel access solutions for 5G new radio," *Proceding of IEEE Wireless Communications and Networking Conference-Workshop*, Marrakech, Morocco, pp. 1-6, 2019.

[12] F. Okewole, A. Ayorinde, S. Adekola, A. Mowete, "A hybrid-analytical-model for the paraboloidal reflector antenna," *Jordan Journal of Electrical Engineering*, vol. 6, no. 4, pp. 348-361, 2020.

[13] S. Lee, S. Hyeon, J. Kim, H. Roh, W. Lee, "The useful impact of carrier aggregation: a measurement study in south korea for commercial LTE-advanced networks," *IEEE Vehicular Technology Magazine,* vol. 12, no. 1, pp. 55-62, 2017.

[14] Y. Huo, X. Dong, W. Xu, M. Yuen, "Enabling multi-functional 5G and beyond user equipment: a survey and tutorial," *IEEE Access*, vol. 7, pp. 116975-117008, 2019.

[15] 3GPP TR 36.850-V11.0.0, *Evolved Universal Terrestrial Radio Access (E−UTRA): Inter-band Carrier Aggregation*, 2013.

[16] E. Tameh, A. Nix, "The use of measurement data to analyse the performance of rooftop diffraction and foliage loss algorithms in a 3-D integrated urban/rural propagation model," *Proceeding of IEEE Vehicular Technology Conference*, Ottawa, Canada, pp. 303-307, 1998.

[17] E. Mellios, Z. Mansor, G. Hilton, A. Nix, J. McGeehan, "Impact of antenna pattern and handset rotation on macro-cell and pico-cell propagation in heterogeneous LTE networks," *Proceeding of IEEE International Symposium on Antennas and Propagation*, Chicago, USA, pp. 1-2, 2012.

[18] A. Doufexi, E. Tameh, A. Nix, S. Armour, A. Molina, "Hotspot wireless LANs to enhance the performance of 3G and beyond cellular networks," *IEEE Communications Magazine,* vol. 41, no. 7, pp. 58-65, 2003.

[19] 3GPP TS 36.942-V10.2.0, *Evolved Universal Terrestrial Radio Access (E−UTRA): Radio Frequency (RF) System Scenarios*, 2010.

[20] 3GPP R1-03-1298, *Effective SIR Computation for OFDM System-Level Simulations*, 2003.

[21] A. Ameen, E. Mellios, A. Doufexi, N. Dahnoun, A. Nix, "LTE-advanced downlink THR evaluation in the 3G and TV white space bands," *Proceeding of IEEE International Symposium on Personal Indoor and Mobile Radio Communications*, London, UK, pp. 771-775, 2013.

[22] K. Beh, A. Doufexi, S. Armour, "Performance evaluation of hybrid ARQ schemes of 3GPP LTE OFDMA system," *Proceeding of International Symposium on Personal Indoor and Mobile Radio Communications*, Athens, Greece, pp. 1-5, 2007.

[23] R. Furukura, K. Honda, K. Ogawa, "A measurement method of MIMO channel capacity considering the base station correlation in 3D MIMO-OTA," *Proceeding of International Workshop on Electromagnetics: Applications and Student Innovation Competition*, Nagoya, Japan, pp. 1-2, 2018.